Mathematical Description and Computer Simulation of Retinal Cometlike Afterimages: A Modified Neural Equation with Stability Analysis

GÁBOR HORVÁTH
Biophysics Group, KFKI Research Institute for Particle and Nuclear Physics, Hungarian Academy of Sciences; H-1525 Budapest, P.O. Box 49, Hungary

ÁRPÁD SZAKÁL
Computer and Automation Institute of the Hungarian Academy of Sciences, Budapest, Hungary

AND

PÉTER ÉRDI
Biophysics Group, KFKI Research Institute for Particle and Nuclear Physics, Hungarian Academy of Sciences; H-1525 Budapest, P.O. Box 49, Hungary

Received 10 October 1991; revised 5 August 1992

ABSTRACT

A mathematical model for the spatiotemporal description of a well-known psychophysical phenomenon, the cometlike afterimage effect (CLAIE), is presented. The CLAIE occurs when a bright circular light spot moves slowly in the peripheral human retina. Under these conditions, the leading edge of the dot looks circular, but the trailing edge becomes elongated like a comet's tail whose length increases with speed and luminance, and the illusion is more prominent for photopic backgrounds. This cometlike motion smear is described on the basis of the temporal responsiveness and adaptation of rods. The model is an extension of an existing neural model of M. N. Oğuztöreli et al., with an additional term that allows prolonged saturation and long decay time following exposure to intense stimuli, and these effects are held responsible for the cometlike smear. The model predicts the response of photoreceptors through a nonlinear ordinary integrodifferential equation, which includes known biophysical terms for response dynamics, adaptation, saturation, and kinetics of intermediate components of the phototransduction process. The introduction of a saturation coefficient into the neural equation makes it possible to distinguish the different saturation thresholds of the rod-and-cone system. Numerical determination of the stationary solutions and complete linear stability analysis of the improved neural equation are given for a neuron of second order, and some computational results are presented for phase flows around different singular points in the phase field. A computer simulation based on the improved neural equation is presented for modeling the development and features of the CLAIE as a function of the speed and

655 Avenue of the Americas, New York, NY 10010 0025-5564/93/$6.00

luminance of the stimulus and the background intensity. The computational results agree well with the psychophysical findings relating to the CLAIE.

1. INTRODUCTION

It is a well-known psychophysical phenomenon that a small circular light spot of high retinal illuminance level has a cometlike appearance when presented moving continuously at low speeds outside the foveal region of the human retina [3]. This perceived lengthening of the circular spot is hereinafter called the cometlike afterimage effect (CLAIE).

In this work a nonlinear mathematical model, which can be interpreted in known biophysical terms, is presented for the spatiotemporal description of the phenomenon of cometlike afterimage effects. The model is based on the neural equation developed by Ŏguztöreli et al. [9, 10, 13, 14]. Although the Oğuztöreli model can describe some well-known visual phenomena [10], the photopic retinal afterimage visual illusions (the CLAIE, for example) based on prolonged saturation and slow temporal relaxation of the response of photoreceptors are beyond the scope of this model.

After a brief sketch of the neurobiological and psychophysical background of the CLAIE, the photopic retinal afterimage phenomenon is studied theoretically and computationally within the scope of Oğuztöreli's neural model. First the insufficiency of the original Oğuztöreli neural equation for describing cometlike afterimages is demonstrated. Then the neural equation is complemented by an additional term, which is responsible for the prolonged saturation and long decay time of the response of photoreceptors. Furthermore, a new saturation coefficient is introduced into the equation, which makes it possible to distinguish the different saturation thresholds of the retinal rod-and-cone system.

The effect of this additional term of the temporal behavior of an isolated photoreceptor is theoretically and computationally studied. A computer simulation based on the modified neural equation is presented for the spatiotemporal description of the development and features of cometlike afterimages as a function of the speed and luminance of the stimulus and background intensity. Finally, in the Appendix, numerical determination of the stationary solutions and complete linear stability analysis of the improved neural equation are given for a neuron of second order, and some computational results are presented for phase flows around different singular points in the phase field.

2. COMETLIKE AFTERIMAGE EFFECT: PSYCHOPHYSICAL BACKGROUND

Electrophysiological measurements of rod receptor potential and intracellular recordings from receptor cells [4, 11] and direct photocurrent measurements in isolated rod receptors [1, 8] show that when the stimulus intensity becomes sufficiently large, the response of rod receptors at a given stimulus duration saturates in amplitude and any further increase in intensity results in prolonged saturation and unusually long decay times after the offset of the stimulus. Slow movements of the retinal image do not cause a distortion of stimulus shape or a significant loss of spatial resolution over a considerable range of target speeds due to the time-resolving ability of the cone system [5].

An exception to this rule can be observed when a small ($\sim 0.5^\circ$ in diameter) circular light spot of high retinal illuminance level moves continuously at a speed as low as $\sim 0.3^\circ/s$, outside the foveal region of the human retina. Although the leading edge of the moving spot remains circular and is spatially well defined, its trailing edge extends into a long tail, which gives the spot a cometlike appearance. The length of the perceived comet increases with the retinal illuminance of the spot.

The parametric variation and the retinal distribution of the CLAIE for different light spot and background stimulus conditions were comprehensively investigated experimentally by Barbur et al. [3]. The CLAIE is no longer seen for retinal illuminance levels of the spot stimulus that are either below a certain threshold value (~ 3 log trolands; 1 troland $\equiv 1$ W/deg^2) or less than the background field. Although the CLAIE is also present at very low background retinal illuminance levels, the strongest effect occurs when the test stimulus is presented against a background field of 2–3 log trolands, which is normally associated with photopic conditions of light adaptation.

Changes in the spectral content of the stimulus or the background field has little or no effect on the retinal distribution of the CLAIE, which is only detected for wavelengths around the middle of the visible spectrum; this spectral region stimulates well both rod and red/green cone receptors. The increment threshold data show clear separation of spectral mechanisms and therefore the involvement of cone receptors too [3].

The two distinct features of cometlike afterimages, the sharp circular leading edge and the extended cometlike trailing edge, are observed only for very low speeds of movement, and in this velocity range the length of the comet tail increases with the speed of movement. For velocities greater than 3°/s these two characteristic features are gradu-

ally degraded, and at higher speeds the stimulus becomes an elongated spot. The CLAIE is seen even for stimulus speeds that are close to the absolute threshold limits for motion detection [2]. These observations suggest that the comet effect reflects very long decay times normally not associated with photopic vision [3].

3. PHOTOPIC RETINAL AFTERIMAGES WITHIN THE SCOPE OF OĞUZTÖRELI'S NEURAL MODEL: DEMONSTRATION OF INSUFFICIENCY OF THE ORIGINAL EQUATION

In a series of papers a general neural model has been developed and studied from a physiological, mathematical, and computational point of view by Oğuztöreli et al. [9, 10, 13, 14]. This neural network model is especially applied for modeling and simulating the vertebrate retina [9] and for some visual phenomena [10]. In this section we demonstrate that photopic retinal afterimages (e.g., the CLAIE) cannot be described within the scope of the original version of this model.

The continuous-time discrete-state space deterministic model [10] is defined by a system of nonlinear ordinary integrodifferential-difference equations of the form

$$\frac{1}{a_{i0}}\frac{dX_i(t)}{dt} + X_i(t) = S\left\{f_i(t) + \sum_{j=1}^{n} c_{ij}X_j(t-\sigma_{ij}) + \sum_{k=1}^{m_i} b_{ik}\int_0^t X_i(\tau)e^{-a_{ik}(t-\tau)}\,d\tau\right\} \qquad (1)$$

for the ith neuron, where t (>0) denotes time; n is the number of neurons in the network; m_i+1 is the "order" of the ith neuron, which gives the number of differential equations after (1) is transformed into the corresponding system of ordinary differential equations (see Section 4.4); $X_i(t)$ is the time-dependent normalized ($0 \leqslant X_i \leqslant 1$) electrical response or activity of the ith neuron; $f_i(t)$ denotes the time-dependent input to the ith neuron; a_{i0} (>0) is the rate constant characterized by a step change in input to the ith neuron producing an exponential approach from the initial value $X_i(0)$ to a steady-state value ξ_i with the rate constant a_{i0}; a_{ik} (>0) is a rate constant for the ith neuron; b_{ik} is an adaptation or self-inhibition factor for the ith neuron when $b_{ik}<0$ and is a self-excitation factor when $b_{ik}>0$ with the rate constant $a_{ik}>0$; c_{ij} is the interaction coefficient between the ith and jth neurons representing inhibition when $c_{ij}<0$ and excitation when $c_{ij}>0$; if the jth neuron is not connected directly to the ith neuron then

$c_{ij} = 0$. $c_{ii} = 0$ for $i = 1,2,\ldots,n$ since the self-inhibition and self-excitation in the ith neuron are characterized by the parameters b_{ik} and a_{ik}; σ_{ij} ($\geqslant 0$) is the time lag of the ith neuron occurring in the transfer of the response of the jth neuron to the ith one; $\sigma_{ii} = 0$ for $i = 1,\ldots,n$; and $S\{u\} = 1/(1+e^{-u})$ is the normalized ($0 \leqslant S \leqslant 1$) neural transfer function that describes the fact that the response of a neuron saturates with large inputs because of its refractory period.

Photopic retinal afterimages (the CLAIE, for example) reflect prolonged saturation of rod responses and extremely long decay times after intense stimuli. Some aspects of the temporal behavior of an isolated photoreceptor can be described well [9, 10, 13, 14] by the original Oğuztöreli neural equation (OONE) of the form

$$\frac{1}{a_0}\frac{dX(t)}{dt} + X(t) = S\left\{f(t) + \sum_{k=1}^{m} b_k \int_0^t X(\tau) e^{-a_k(t-\tau)}\, d\tau\right\}. \quad (2)$$

In Figure 1 the results of a numerical simulation can be seen for a photoreceptor described by the OONE (2), the numerical solution of which is performed by the method of Gottwald and Wanner [6]. We progressively increased the amplitude f_s (Figure 1A) and duration T (Figure 1B) of a rectangular input at zero background intensity $f_b = 0$ (moving light spot in darkness). Figure 1A shows that if one increases the amplitude of the input, the photoreceptor saturates above a critical value of f_s; however, this saturation comes to an end as soon as the intense stimulus finishes, and the response quickly decreases with a short decay time. Similar temporal behavior can be seen in Figure 1B; that is, in spite of the increase of the external stimulus duration T, the saturated response of the photoreceptor decreases immediately and rapidly after the end of the intense stimulus.

Taking this simulation into account and analyzing (2), one can establish that prolonged saturation characterized by increasing saturation time due to increasing amplitude and/or duration of the intense input and extremely long decay time cannot occur in the temporal behavior of a photoreceptor described by the OONE. The reason for this is that the end of the input $f(t)$ in (2) results in a steplike decrease in the argument of the transfer function $S\{u\}$, thereby immediately producing an exponential approach with rate constant a_0 in the response $X(t)$ of the photoreceptor from the saturated value 1 to a smaller steady-state value.

Consequently the OONE is insufficient for describing photopic retinal afterimages characterized by prolonged saturation and long decay time of the response of photoreceptors induced by intense stimuli. In

the following section we show a possible way to improve (2) in order to be able to describe the phenomenon of photopic retinal afterimages.

4. IMPROVED NEURAL EQUATION

4.1. *SATURATION COEFFICIENT*

Bearing in mind the photopic retinal afterimages, the most important difference between rods and cones is their different response amplitudes to a single photon. To describe mathematically the characteristic difference between the critical input amplitude required to produce saturation in rod and cone receptors, a new saturation coefficient ω must be introduced into the neural transfer function $S\{u\}$ as follows:

$$\check{S}\{u, \omega\} := \frac{1}{1 + e^{-u/\omega}}, \qquad \omega > 0. \tag{3}$$

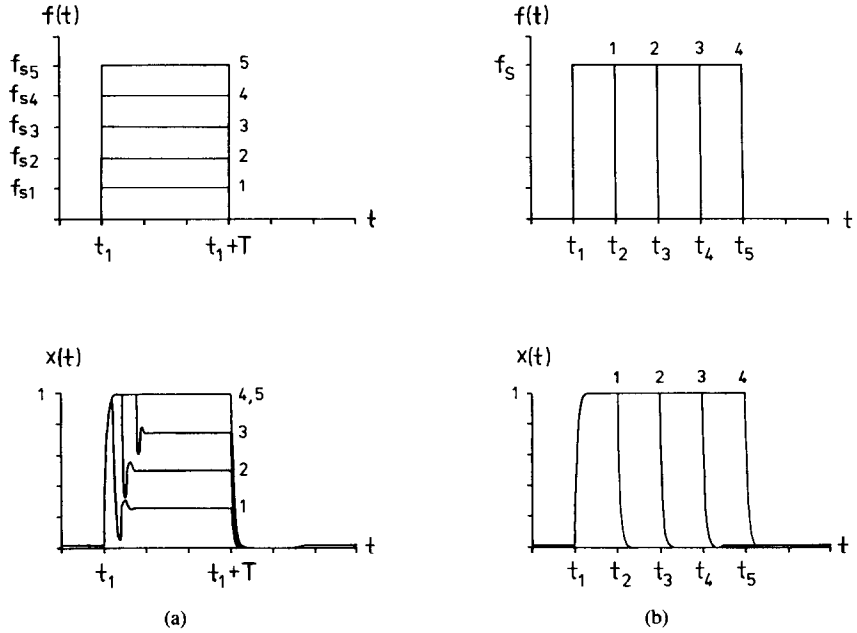

FIG. 1. Normalized responses $X(t)$ of an isolated second-order $(m+1=2)$ retinal photoreceptor described by the OONE (2) with the parametric configuration $a_0 = 100\ \mathrm{s}^{-1}$, $a_1 = 15\ \mathrm{s}^{-1}$, $b_1 = -2000\ \mathrm{s}^{-1}$ to a series of rectangular external inputs $f(t)$ of increasing amplitude f_s (a) and duration T (b) at zero background intensity $f_b = 0$ (moving light spot in darkness). (a) $t_1 = 200$ ms, $T = 600$ ms, $f_{si} = i\,\Delta f_s$, $i = 1,\ldots,5$, with $\Delta f_s = 40$; (b) $t_1 = 200$ ms, $f_s = 200$, $t_j = t_1 + (j-1)\Delta T$, $j = 1,\ldots,5$, with $\Delta T = 200$ ms. It can be seen that there is neither prolonged saturation nor slow temporal relaxation of the response.

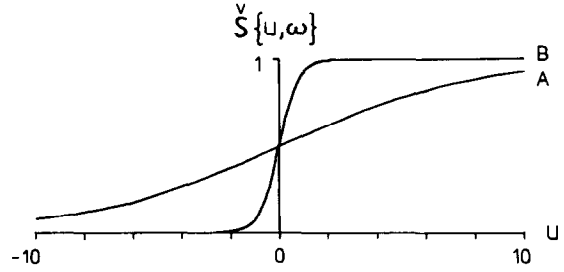

FIG. 2. Graph of neural transfer function $\check{S}\{u, \omega\}$ for large ($\omega_A = 4$) and small ($\omega_B = 0.4$) values of the saturation coefficient ω. (A, B) Transfer functions of retinal cones and rods, respectively, in accordance with relation $\omega_{\text{rod}} \ll \omega_{\text{cone}}$.

The transfer function is the saturation stage of the model presented through which the transduction cascade passes before driving the response up. In Figure 2 the graph of $\check{S}\{u, \omega\}$ is shown for a large (curve A) and a small (curve B) value of ω. On the basis of (2) and (3), one can see that a photoreceptor with large ω saturates only for much larger external input amplitudes than a receptor with smaller ω. So retinal rod cells can be characterized by a much smaller saturation coefficient ω_{rod} than the cone cells (ω_{cone}), that is,

$$\omega_{\text{rod}} \ll \omega_{\text{cone}}. \tag{4}$$

4.2. *STIMULUS HISTORIC TERM RESPONSIBLE FOR PROLONGED SATURATION AND LONG DECAY TIME OF RETINAL PHOTORECEPTORS*

Photochemical Background. In darkness a photoreceptor has an appreciable permeability to Na^+ ions, which flow into the outer segment of the receptor. This inward current is balanced by the outward current of K^+ ions from the rest of the cell. When the rhodopsin molecules of a photoreceptor absorb light, the influx of Na^+ ions is blocked, thereby reducing the dark current and resulting hyperpolarization of the transmembrane [12].

In the dark the photoreceptors have a high concentration of cyclic guanosine monophosphate (cGMP), a substance that binds to pores in the surface membrane and opens them, allowing Na^+ ions to enter. In the light the concentration of cGMP drops, cGMP leaves the binding sites, and the pores close [15].

Three main steps intervene between the excitation of rhodopsin and the enzymatic cleavage of cGMP. When one of the two components of rhodopsin, retinal, absorbs a photon and the other component, opsin, is activated, rhodopsin in turn activates the enzyme tranducin. Transducin then activates a specific phosphodiesterase, which then opens the ring of cGMP by hydrolysis. The system behaves like a chemical photomultiplier: absorption of a single photon by rhodopsin causes the rapid breakdown of hundreds of cGMP molecules and blocks the entry of a million Na^+ ions. Upon an increase in the light intensity, more and more cGMP molecules progressively break down, as a consequence of which more and more pores close, until finally all the pores close. At this stage there is total saturation of the photoreceptor [12, 15].

Stimulus Historic Term. An appropriate mathematical formulation of the above photochemical saturation phenomena is to add a convolution integral term

$$\mathrm{SHT}(t) := \int_{t_0}^{t} f(\tau)\,\mathrm{SK}(t-\tau)\,d\tau, \tag{5a}$$

where

$$\mathrm{SK}(\tau) := \sum_{l=1}^{M} c_l e^{-\varphi_l \tau} \geqslant 0, \tag{5b}$$

to the argument of the neural transfer function $\check{S}\{u, \omega\}$ in (2). This term contains a sum proportional to the input (light intensity) and exponential factors with rate constants φ_l and coefficients c_l, where time t_0 is the beginning of the stimulation and function $\mathrm{SK}(\tau)$ represents an M-step photochemical reaction kinetics underlying the chemical photomultiplier mechanism of the prolonged saturation of photoreceptors. Function $\mathrm{SHT}(t)$ is proportional to the time-dependent concentration of the enzyme (activated by transducin molecules) cleaving cGMP, an enzyme that tunes the closing of pores and the blocking of the influx of Na^+ ions to a brief flash. So the function $\mathrm{SK}(\tau)$ tunes the saturation of photoreceptors; therefore we call it the saturation kernel.

Since term (5a) also depends on the earlier values of the input function $f(\tau)$, in exponentially decreasing temporal participation—that is, on the history of the stimulus—we call it the stimulus historic term. Equations (5a) and (5b) are related only to stimulus. This makes the historic term a "feedforward" mechanism rather than a feedback mechanism. The biophysical motivation for using multiple exponential terms in the function $\mathrm{SK}(\tau)$ is explained in Section 4.3.

The final form of the improved Oğuztöreli neural equation (IONE) is

$$\frac{1}{a_0}\frac{dX(t)}{dt} + X(t) = \left[1 + \exp\left\{\frac{-f(t) - \sum_{k=1}^{m} b_k \int_{t_0}^{t} X(\tau) e^{-a_k(t-\tau)}\, d\tau - \sum_{l=1}^{M} c_l \int_{t_0}^{t} f(\tau) e^{-\varphi_l(t-\tau)}\, d\tau}{\omega}\right\}\right]^{-1} \quad (6)$$

If there is an appropriate parametric configuration, the stimulus historic term ensures that the argument of the neural transfer function $\check{S}\{u, \omega\}$ remains above the critical value required to produce saturation for a time that increases with the amplitude and/or duration of intense stimuli. Then it decreases very slowly after the stimuli stop. So the stimulus historic term can ensure prolonged saturation and extremely long decay time of the response of a photoreceptor cell, as will be shown later.

4.3. *SATURATION KERNEL*

If the function $SK(\tau)$ in the form of (5b) has the schematic graph as represented in Figure 3 [that is, $SK(\tau)$ rapidly reaches its maximum value at τ^*, after which it relaxes slowly], then its convolution $SHT(t)$

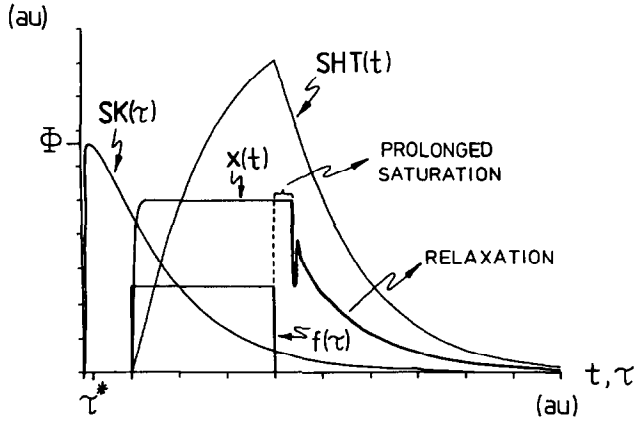

FIG. 3. If the saturation kernel $SK(\tau)$ in the IONE (6) has the schematic graph shown, then its temporal convolution with a rectangular input $f(\tau)$, namely, the stimulus historic term $SHT(t)$, can ensure the prolonged saturation and the slow temporal relaxation of the response $X(t)$ of a neuron after the intense stimuli cease. au, arbitrary unit.

with input ensures the prolonged saturation and extremely long decay time of the response $X(t)$ of a neuron after the end of intense stimuli for an appropriate parametric configuration. On the basis of Figure 3 one can write

$$\mathrm{SK}(0) = \sum_{l=1}^{M} c_l = 0, \tag{7}$$

$$\mathrm{SK}(\tau^*) = \sum_{l=1}^{M} c_l e^{-\varphi_l \tau^*} = \Phi > 0, \tag{8}$$

$$\left[\frac{d\mathrm{SK}(\tau)}{d\tau}\right]_{\tau=\tau^*} = -\sum_{l=1}^{M} c_l \varphi_l e^{-\varphi_l \tau^*} = 0. \tag{9}$$

Since the photochemical mechanism (the chain of molecular events leading to the reduction of cGMP) underlying the saturation of retinal photoreceptors consists of three steps [12, 15], the case $M = 3$ seems to be appropriate for the term $\mathrm{SHT}(t)$ in the IONE (6). Using (7)–(9), three parameters can be determined from among the parameters $\{c_l, \varphi_l\}$ $(l = 1,\ldots, M)$ of the function $\mathrm{SK}(\tau)$. From (7)–(9), one can obtain for the vector $\boldsymbol{c} = (c_1, c_2, c_3)$,

$$\boldsymbol{c} = \frac{\Phi}{K}(\boldsymbol{e} \times \boldsymbol{v}),$$

$$K = E_1 E_2(\varphi_1 - \varphi_2) + E_3 E_1(\varphi_3 - \varphi_1) + E_2 E_3(\varphi_2 - \varphi_3),$$

$$e_i = 1, \qquad v_i = \varphi_i E_i, \qquad E_i = e^{-\varphi_i \tau^*}, \qquad i = 1,2,3. \tag{10}$$

4.4. *STATIONARY SOLUTIONS*

If one introduces the quantities

$$Y_k(t) := \int_{t_0}^{t} X(\tau) e^{-a_k(t-\tau)}\, d\tau, \qquad k = 1,\ldots, m, \tag{11}$$

the nonlinear ordinary integrodifferential equation (6) can be transformed into the following system of ordinary differential equations:

$$\frac{dX(t)}{dt} = -a_0 X(t) + a_0 \check{S}\left\{f(t) + \sum_{k=1}^{m} b_k Y_k(t) + \mathrm{SHT}(t), \omega\right\},$$

$$\frac{dY_k(t)}{dt} = X(t) - a_k Y_k(t), \qquad X(t_0) = X_0,$$

$$Y_k(t_0) = Y_{k0} = 0, \qquad k = 1,\ldots, m. \tag{12}$$

After this transformation, (6) has the following form in the stationary case, that is, when $t \to \infty, dX/dt = dY_k/dt = 0, f(t) = f_0 = \text{constant}$:

$$G(\xi) \equiv 1 - \frac{1}{\xi} + \exp\left\{\frac{-\left[1+\sum_{l=1}^{M}(c_l/\varphi_l)\right]f_0 - \xi\sum_{k=1}^{m}(b_k/a_k)}{\omega}\right\} = 0,$$
$$\xi_k = \xi/a_k, \qquad k = 1,\ldots,m, \tag{13}$$

where ξ and ξ_k represent the stationary values of $X(t)$ and $Y_k(t)$, respectively. One can see from (13) that the new introduced term SHT(t) modulates only the dynamics of a neuron so that the stationary solution ξ of (6) is the same as that of (2) if

$$\sum_{l=1}^{M}\frac{c_l}{\varphi_l} = 0. \tag{14}$$

The numerical determination of the stationary solutions and complete linear stability analysis of the IONE are given in the Appendix for a neuron of second order ($m+1=2$). Some computational results for phase flows around different singular points in the phase field of the OONE and the IONE can be seen in Figures 11–13 (see Appendix).

5. PROLONGED SATURATION AS A SOLUTION OF THE IMPROVED NEURAL EQUATION

Consider an isolated retinal photoreceptor described by the IONE (6) and stimulated by the rectangular input

$$\begin{aligned} f(t_0 \leqslant t \leqslant t_1) &= f_b && \text{(background)},\\ f(t_1 < t < t_1 + T \equiv t_2) &= f_s && \text{(spot)},\\ f(t_2 \leqslant t) &= f_b && \text{(background)}, \end{aligned} \tag{15}$$

which corresponds to a moving light spot of strength f_s at background intensity f_b. In this case the stimulus historic term has the form

$$\begin{aligned} \text{SHT}(t_0 \leqslant t \leqslant t_1) &= f_b\sum_{l=1}^{M}\frac{c_l}{\varphi_l}\left[1 - e^{-\varphi_l(t-t_0)}\right],\\ \text{SHT}(t_1 < t < t_2) &= \sum_{l=1}^{M}\frac{c_l}{\varphi_l}e^{-\varphi_l t}\left[f_b(e^{\varphi_l t_1} - e^{\varphi_l t_0}) + f_s(e^{\varphi_l t} - e^{\varphi_l t_1})\right],\\ \text{SHT}(t_2 \leqslant t) &= \sum_{l=1}^{M}\frac{c_l}{\varphi_l}e^{-\varphi_l t}\left[e^{\varphi_l t_1}(f_s - f_b)(e^{\varphi_l T} - 1) + f_b(e^{\varphi_l t} - e^{\varphi_l t_0})\right]. \end{aligned} \tag{16}$$

In the limit $t_0 \to -\infty$, the stimulus historic term has the simpler form

$$\lim_{t_0 \to -\infty} \mathrm{SHT}(t_0 \leqslant t \leqslant t_1) = f_b \sum_{l=1}^{M} \frac{c_l}{\varphi_l},$$

$$\lim_{t_0 \to -\infty} \mathrm{SHT}(t_1 < t < t_2) = \sum_{l=1}^{M} \frac{c_l}{\varphi_l}\left[f_s - (f_s - f_b)e^{-\varphi_l(t-t_1)}\right],$$

$$\lim_{t_0 \to -\infty} \mathrm{SHT}(t_2 \leqslant t) = \sum_{l=1}^{M} \frac{c_l}{\varphi_l}\left[e^{\varphi_l t_1}(e^{\varphi_l T} - 1)(f_s - f_b)e^{-\varphi_l t} + f_b\right]. \quad (17)$$

If $f_b = 0$ (stimulation in darkness), one can obtain from (17)

$$\lim_{t_0 \to -\infty} \mathrm{SHT}(t_1 + T) = \sum_{l=1}^{M} \frac{c_l}{\varphi_l} f_s(1 - e^{-\varphi_l T}). \quad (18)$$

Analyzing (18), one can realize that factors $f_s[1 - \exp(-\varphi_l T)]$, $l = 1,2,3$, can ensure the prolonged saturation due to stimuli in darkness, because on the one hand the value of $\mathrm{SHT}(t_1 + T)$ increases proportionally to the stimulus intensity f_s, and on the other hand it increases exponentially with the duration T of the stimulus. Therefore, the larger the argument of $\check{S}\{u, \omega\}$ at the moment the input stops $[f(t)_{\mathrm{off}} = 0]$, the larger the amplitude f_s and/or duration T of the stimulus. As a consequence of this, solution $X(t)$ of (6) remains for a while at the saturated maximum value 1 following the exposure to intense stimuli. This effect is the prolonged saturation. Then $X(t)$ decreases only very slowly with extremely long decay time.

In Figure 4 some results of a numerical simulation can be seen for the above photoreceptor. We progressively increased the amplitude and duration of the rectangular input in the same way as in Figures 1A and 1B, respectively. Figure 4A shows that on an increase in the amplitude f_s of the stimulus, the photoreceptor saturates above a critical amplitude, and this saturation does not come to an end immediately after the stop (at time $t = t_1 + T$) of the intense stimulus; in other words, it is prolonged. The saturation time increases progressively with the amplitude of the stimulus. An additional temporal feature is that the response decreases with a long decay time following the saturation. Similar temporal behavior can be seen in Figure 4B; that is, if the stimulus duration T is increased, the saturation time increases progressively after the end of the intense stimulus.

The retinal photoreceptor system needs a certain time for adaptation to a given background intensity, as is well known from psychophysics and physiology [12, 15]. During this adaptation period the response of photoreceptors reaches its steady state corresponding to the back-

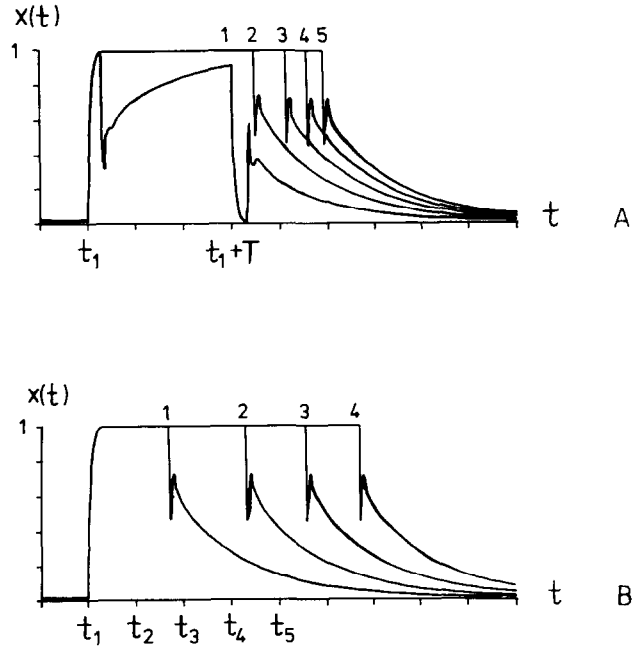

FIG. 4. Responses of an isolated second-order ($m+1=2$) retinal photoreceptor described by the IONE (6) with the parametric configuration $a_0 = 100\ s^{-1}$, $a_1 = 15\ s^{-1}$, $b_1 = -2000\ s^{-1}$, $\varphi_1 = (2\ ms)^{-1}$, $\varphi_2 = (80\ ms)^{-1}$, $\varphi_3 = (300\ ms)^{-1}$, $\tau^* = 18$ ms, $\Phi = 7.5\ s^{-1}$, $\omega = 1$ to a series of rectangular inputs of increasing amplitude f_s (A) and duration T (B) at zero background intensity $f_b = 0$ in the same way as those of Figures 1A and 1B, respectively. It is evident in both cases that prolonged saturation and slow temporal relaxation occur.

ground illuminance conditions. During the computer modeling of the response of photoreceptors investigated, one can simulate this adaptation in the following two ways.

(1) One takes an arbitrary initial value X_0 for variable $X(t)$ with $t_0 \ll t_1$ in (16) and solves numerically the system of ordinary differential equations (12) with $f(t) = f_b = \text{constant}$ until $X(t)$ approaches its stationary value $\xi(f_b)$. After this adaptation procedure one can begin the effective simulation for input (15) using (16).

(2) One first solves numerically the transcendental equation (13) for $\xi(f_b)$ and then begins the simulation at time $t = 0$, solving (12) with $X(0) = \xi(f_b)$ and $Y_k(0) = \xi(f_b)/a_k$, $k = 1,\ldots,m$, for input (15) using (17). In this case one spares the adaptation period, replacing it by the quicker calculation of $\xi(f_b)$.

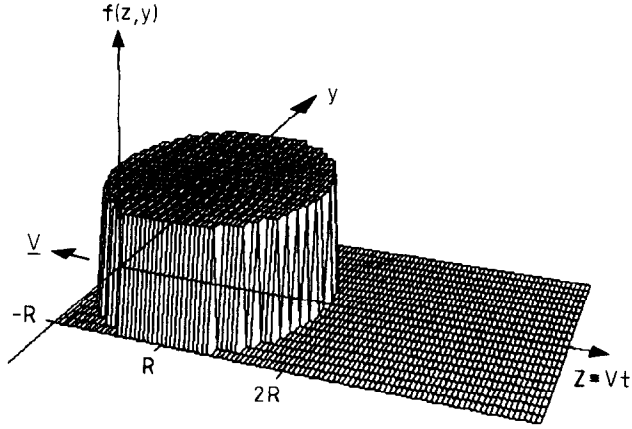

FIG. 5. Intensity function $f(z = vt, y)$ of a circular light spot moving with velocity vector v in the opposite direction to axis z as an external input of the two-dimensional retinal photoreceptor system investigated. R is the radius of the spot.

6. SPATIOTEMPORAL DESCRIPTION OF THE CLAIE

6.2. *SPATIAL ACTIVITY PATTERN INDUCED BY A MOVING LIGHT SPOT IN DARKNESS*

To determine how the retinal image of a moving circular light spot of high retinal illuminance level becomes distorted, let us investigate the spatial activity pattern induced by this stimulus in a model retina. Consider a two-dimensional retinal rod system, the individual photoreceptor cells of which are isolated lying in the $(z = vt, y)$ plane of Figure 5. The spot moves with velocity vector v in the opposite direction to axis z. First we investigate a moving light spot in darkness, that is, at zero background intensity $f_b = 0$. In this case all the rods placed on a line parallel to axis z at distance $|y| \leqslant R$, where R is the radius of the spot, receive the same temporal input,

$$\begin{aligned} f(y,\tau) &= 0 \quad \text{if} \quad \tau < \tau_1(y) \quad \text{or} \quad \tau > \tau_2(y), \\ f(y,\tau) &= f_s \quad \text{if} \quad \tau_1(y) \leqslant \tau \leqslant \tau_2(y), \end{aligned} \tag{19a}$$

where

$$\tau_1(y) = \frac{R - \sqrt{R^2 - y^2}}{v}, \qquad \tau_2(y) = \frac{R + \sqrt{R^2 - y^2}}{v}, \qquad |y| \leqslant R, \tag{19b}$$

and the relative time τ is measured from the moment the front of the spot crosses the abscissa of a given photoreceptor.

Since the temporal response of isolated cells of the rod system investigated lying on a line parallel to axis z is the same (apart from being shifted temporally), the shape of the spatial activity pattern of the system induced by the moving spot does not change temporally (disregarding an initial transition). The spatial activity pattern is shifted on the system only parallel to the velocity vector $\boldsymbol{v}$, so it can be obtained from the series of temporal response functions $X(t)$ of rods placed perpendicularly to the velocity vector $\boldsymbol{v}$, using the transformation $t \rightarrow z \equiv vt$. Some results can be seen in Figures 6 and 7 for a rod system described by the OONE and the IONE, respectively, as a function of parameter $w \equiv v/2R$. One can see that a photoreceptor system described by (2) cannot produce a cometlike afterimage (Figure 6), but a system based on (6) can (Figure 7).

6.2. *INFLUENCE OF THE BACKGROUND ON THE CLAIE*

So far we have investigated the cometlike afterimage effect induced by a moving circular light spot in total darkness, that is, when the background intensity $f_b = 0$. Now we study the influence of f_b on the CLAIE. In Figure 8 the spatial activity pattern can be seen for a series of intensities f_b with the velocity at which the comet tail in darkness is the longest (see Figure 7B) for a given f_s. Figure 8 shows that if the background intensity f_b ($< f_s$) is increased, the cometlike afterimage becomes more developed, and the comet tail increases progressively; however, for larger values of f_b the elongated spatial activity pattern merges gradually into the background and loses its cometlike appearance.

6.3. *INFLUENCE OF THE STIMULUS AMPLITUDE ON THE CLAIE IN DARKNESS*

The precondition for cometlike afterimages is the appropriately high retinal illuminance level of the moving circular light spot. Therefore it is worth investigating the influence of the stimulus amplitude f_s on the CLAIE in order to answer the question: How does the cometlike afterimage develop in darkness when the illuminance level of the light spot increases gradually at a given velocity? Some results are shown in Figure 9. One can see that on gradually increasing the stimulus strength, the cometlike afterimage forms above a certain value of f_s (Figure 9E) and becomes more characteristic; it then turns into an elongated spot (Figure 9G) for very intense stimuli.

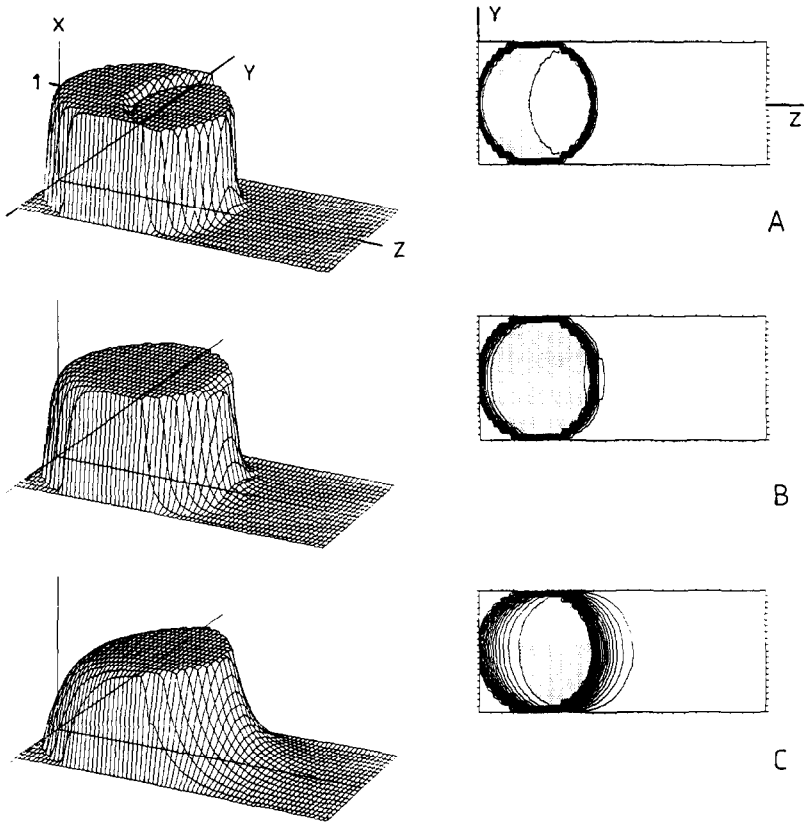

FIG. 6. Spatial activity pattern (SAP) of a retinal rod system described by the OONE (2) as a function of parameter $w \equiv v/d$, where v is the velocity of the light spot of diameter $d = 1$ mm. Parametric configuration: $a_0 = 100\ s^{-1}$, $a_1 = 12.5\ s^{-1}$, $b_1 = -4000\ s^{-1}$, $f_s = 300$, $f_b = 0$. Left: Three-dimensional view of the SAP. Right: Two-dimensional contour map generated by intersecting the SAP by a series of planes parallel with the (y, z) plane. The plateau (dotted) represents the saturation of the photoreceptor system. (A) $w = 2\ s^{-1}$, (B) $w = 4\ s^{-1}$, (C) $w = 12\ s^{-1}$. In spite of the saturation of the photoreceptors, prolonged saturation and slow relaxation underlying the CLAIE do not occur.

7. DISCUSSION AND CONCLUSIONS

In this work a special, cometlike photopic retinal afterimage effect is theoretically and computationally investigated. Photopic retinal afterimages are characterized by prolonged saturation with increasing saturation time due to increasing amplitude and/or duration of the intense input and extremely long decay time of rod responses after stimuli of

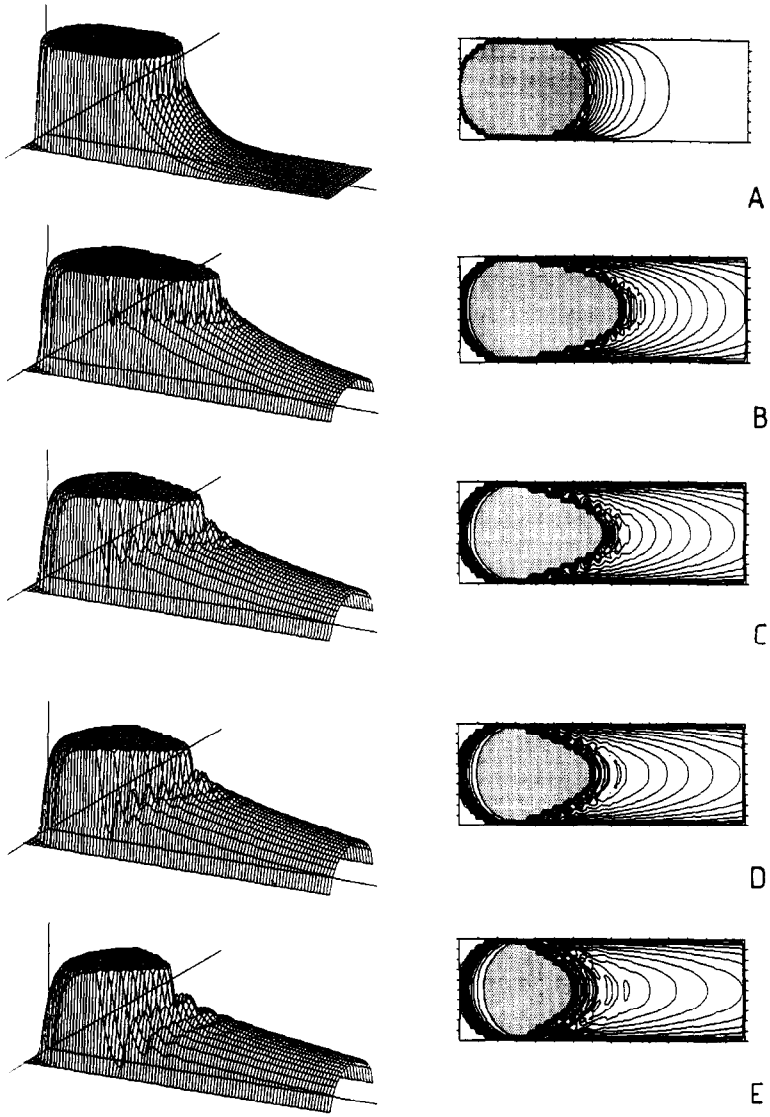

FIG. 7. Spatial activity pattern for a rod system described by the IONE (6) with the parametric configuration $a_0 = 100\ s^{-1}$, $a_1 = 12.5\ s^{-1}$, $b_1 = -4000\ s^{-1}$, $\omega = 1$, $\Phi = 8\ s^{-1}$, $\tau^* = 18$ ms, $\varphi_1 = (2\ \text{ms})^{-1}$, $\varphi_2 = (80\ \text{ms})^{-1}$, $\varphi_3 = (300\ \text{ms})^{-1}$, $f_s = 300$, $f_b = 0$. (A) $w = 1\ s^{-1}$, (B) $w = 4\ s^{-1}$, (C) $w = 6\ s^{-1}$, (D) $w = 7\ s^{-1}$, (E) $w = 9\ s^{-1}$. The prolonged saturation and slow relaxation of the photoreceptors responsible for the CLAIE can be well seen.

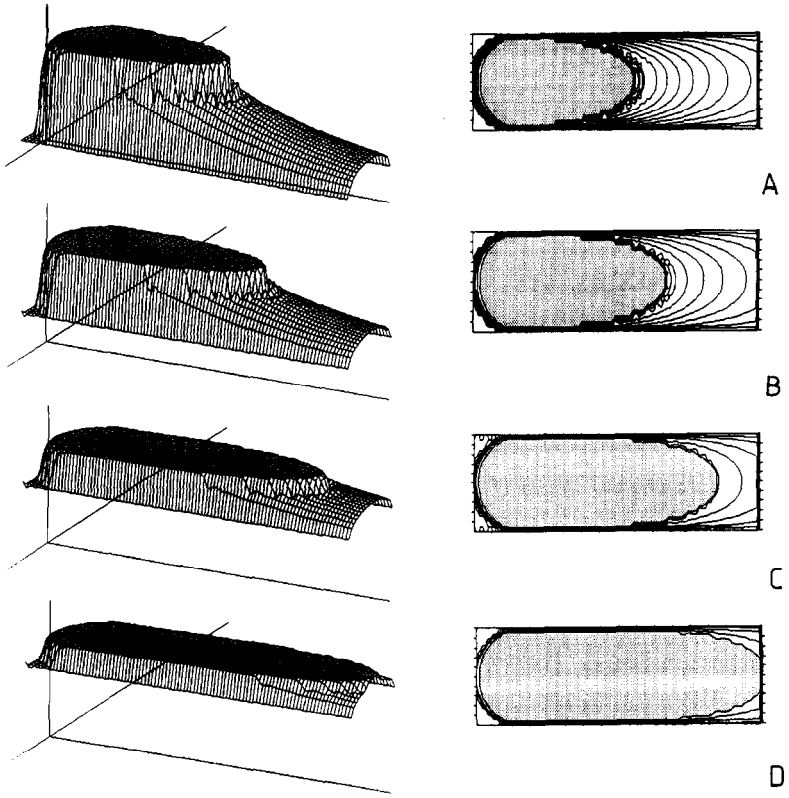

FIG. 8. Spatial activity pattern of the photoreceptor system of Figure 7 with $f_s = 300$ and $w = 4\ s^{-1}$ for a series of background intensities f_b. (A) $f_b = 10$, (B) $f_b = 30$, (C) $f_b = 50$, (D) $f_b = 60$.

high retinal illuminance levels. The cometlike phenomenon has two distinct features: a sharp, circular leading edge and an extended cometlike trailing edge induced by an intense moving circular light spot.

The basis of the mathematical description of the cometlike afterimage effect (CLAIE) is Oğuztöreli's neural model developed for the modeling and simulation of the vertebrate retina. Since prolonged saturation and slow temporal relaxation cannot occur in the temporal behavior of a photoreceptor described by the OONE (2) (Figures 1 and 6), its modification is necessary for describing the CLAIE.

(i) A new saturation coefficient ω is introduced into the neural transfer function (3) to describe the different saturation thresholds of

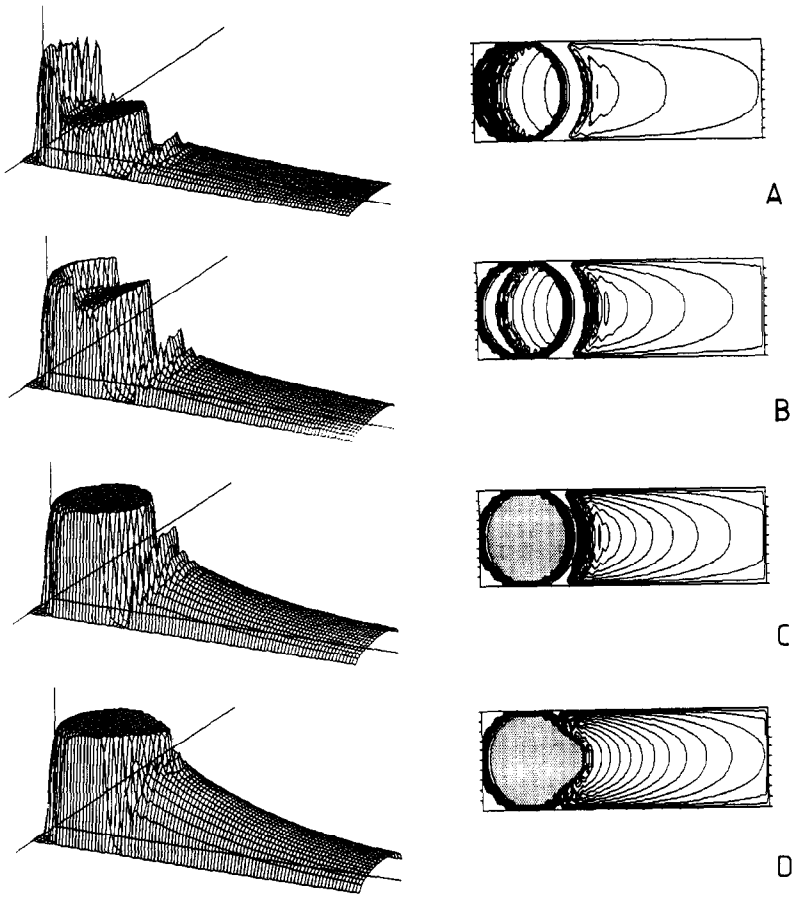

FIG. 9. Spatial activity pattern of the photoreceptor system of Figure 7 with $f_b = 0$ and $w = 4\ s^{-1}$ for a series of stimulus amplitudes f_s. (A) $f_s = 50$, (B) $f_s = 100$, (C) $f_s = 150$, (D) $f_s = 200$, (E) $f_s = 250$, (F) $f_s = 350$, (G) $f_s = 500$.

the input amplitude of retinal rod and cone photoreceptors using the relation $\omega_{rod} \ll \omega_{cone}$.

(ii) A new additional term, (5a), called the stimulus historic term (SHT), is introduced into the IONE (6). This term is responsible for the prolonged saturation and long decay time of the response of retinal photoreceptors after intense stimuli. In the stimulus historic term, a saturation kernel SK(τ) (5b) represents the (M=3)-step photochemical reaction kinetics underlying the chemical photomultiplier mechanism (the chain of molecular events leading to reduction of cGMP) of the saturation of photoreceptors.

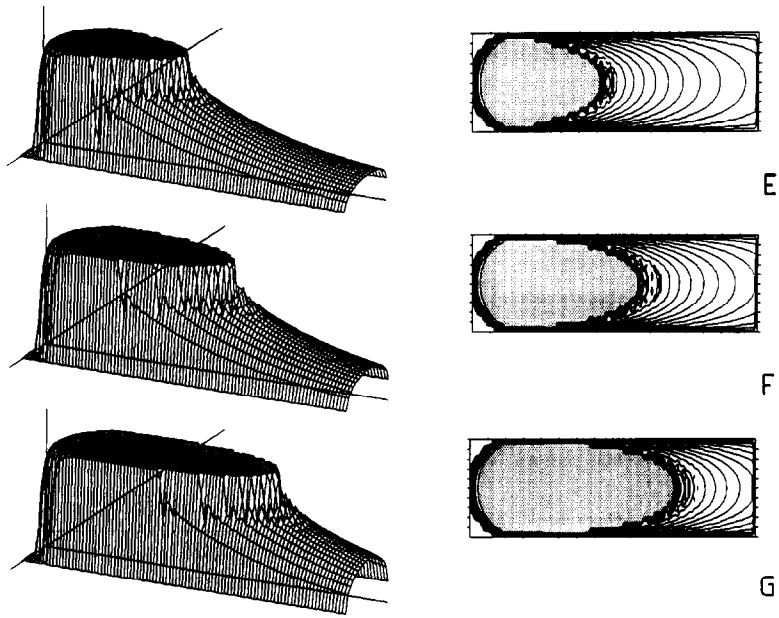

FIG. 9. (*Continued*)

(iii) Under condition (14) the additional stimulus historic term introduced modulates only the dynamics of a neuron; that is, the stationary solutions of the IONE (6) are the same as those of the OONE (2).

The problem of how spatial interaction between receptors influences the results of the present investigation is beyond the scope of this paper. However, Barbur et al. [3] showed that a rod–cone interaction underlies the cometlike afterimages. The effect of the cones on the CLAIE is to sharpen the circular leading edge. This kind of interaction is not considered in this work; we studied the spatiotemporal activity pattern of the retinal rod system only.

Equation (6) is applied to the spatiotemporal description of the CLAIE. The results of our computer simulations are in accordance with the experimental, psychophysical findings of Barbur et al. [3] on the cometlike phenomenon. Barbur et al. [3] also made a model simulation for describing the CLAIE, using a convolution technique. Contrary to their model, our model seeks to describe the cometlike motion smear of moving dots by means of a nonlinear ordinary integrodifferential equation for the response of photoreceptors. Of course, our model can be improved by taking into consideration rod–cone interaction to model

the sharpening effect of the cone system on the circular leading edge of the retinal image of the stimulus, but this is out of the scope of the present paper.

The disadvantage of the Barbur et al. [3] model is that it uses definite temporal response functions to predict the cometeffect, and therefore the model is rigid with respect to the modeling of other visual phenomena. The OONE and the IONE used in this work, however, can describe well a series of well-known visual phenomena [10].

Although one must not preclude the possibility that the cometlike smear also involves postretinal mechanisms, the presented model and the earlier Barbur et al. [3] model demonstrate that the CLAIE can be explained well by retinal mechanisms at the level of photoreceptors; that is, cometlike afterimages may develop in early vision.

The results of our computer simulations based on the IONE (6) are summarized as follows.

(iv) It is shown that prolonged saturation with increasing saturation time and long decay time due to increasing amplitude and/or duration of intense stimuli can occur in the temporal behavior of a photoreceptor described by the IONE (Figures 4 and 7).

(v) The shape distortion of the perceived image of a moving circular light spot of high retinal illuminance level in darkness is studied as a function of its velocity. Distortion of shape is represented by the spatial activity pattern of the retinal rod system (Figure 7). If one increases the velocity v of the light spot, the two distinct features of the cometlike afterimage, the sharp circular leading edge and the extended cometlike trailing edge, gradually develop. The length of the comet tail increases with v. For larger values of v, these characteristic features are gradually degraded and the retinal image becomes an elongated spot (Figure 7).

(vi) The influence of the background intensity f_b on the CLAIE is investigated. On increasing f_b, the comet tail increases progressively, and for larger values of f_b ($< f_s$) the elongated spatial activity pattern merges gradually into the background and loses its cometlike appearance (Figure 8).

(vii) The influence of the stimulus strength f_s on the CLAIE in darkness is studied. On gradually increasing f_s, the cometlike afterimage forms above a certain value of the stimulus amplitude and becomes more characteristic. Eventually it turns into an elongated spot for very intense stimuli (Figure 9).

(viii) The spatial activity pattern of our simulations (Figures 7–9) has a plateau at the level $X(t) = 1$ followed by a slowly relaxing long trail. The plateau and its shape correspond to the cometlike retinal afterimage. The long trail corresponds to the much paler and gradually blurring

elongated smear perceived after every moving intense light spot, which is the most characteristic feature of photopic retinal afterimages [5].

On the basis of the linear stability analysis of the IONE and the computationally determined phase flows around different singular points in the phase field for a second-order neuron ($m+1=2$), the following can be concluded (Appendix, Figure 10–13):

(ix) If $b_1 < 0$, there is always one stationary solution $S(\xi, \xi_1)$ of the IONE (Figures 10 and 12) along the straight line $\xi_1 = \xi / a_1$ in the phase field for a given input f. If $\omega < \tilde{\omega}_c \equiv -a_0 b_1 / (a_1 - a_0)^2$ and $a_1 \neq a_0$, the singular point $S(\xi, \xi_1)$ is an asymptotically stable node if $0 \leqslant \xi < \tilde{\xi}_1$ or $\tilde{\xi}_2 < \xi \leqslant 1$, an asymptotically stable focus if $\tilde{\xi}_1 < \xi < \tilde{\xi}_2$, and an asymptotically stable one-tangent node if $\xi = \tilde{\xi}_1$ or $\xi = \tilde{\xi}_2$, where $\tilde{\xi}_1$ and $\tilde{\xi}_2$ are expressed by (34) (Figure 12). If $\omega = \tilde{\omega}_c$, the region of the asymptotically stable focus disappears in the phase field, and $\tilde{\xi}_1 = \tilde{\xi}_2 = 1/2$. If $\omega > \tilde{\omega}_c$, every singular point is an asymptotically stable node. If $a_1 = a_0$, then $\tilde{\omega}_c = +\infty$, $\tilde{\xi}_1 = 0$, and $\tilde{\xi}_2 = 1$. In this case the points $S_1(\xi = 0, \xi_1 = 0)$ and $S_2(\xi = 1, \xi_1 = 1/a_1)$ are asymptotically stable one-tangent nodes, and every other singular point is an asymptotically stable focus.

(x) If $b_1 > 0$, there are one, two, or three stationary solutions of the IONE positioned on the straight line $\xi_1 = \xi / a_1$ in the phase field for a given input depending on f and ω (Figure 10). If $\omega < \check{\omega}_c \equiv b_1 / 4a_1$, the stationary solution $S(\xi, \xi_1)$ is an asymptotically stable node if $0 < \xi < \check{\xi}_1$ or $\check{\xi}_2 < \xi < 1$, an indifferent singular point if $\xi = \check{\xi}_1$ or $\xi = \check{\xi}_2$, and an unstable saddle point if $\check{\xi}_1 < \xi < \check{\xi}_2$, where $\check{\xi}_1$ and $\check{\xi}_2$ are expressed by (39) (Figure 13). In this case there can be one, two, or three different singular points for a given input depending on f (Figures 10 and 13). If $\omega = \check{\omega}_c$, the region of the unstable saddle point disappears in the phase field, and $\check{\xi}_1 = \check{\xi}_2 = 1/2$. If $\omega > \check{\omega}_c$, every singular point is an asymptotically stable node. In the latter two cases there is always one stationary solution for a given input (Figures 10 and 13). If $a_1 = a_0$ and $\xi = 0$ or $\xi = 1$, the singular points $S_1(\xi = 0, \xi_1 = 0)$ and $S_2(\xi = 1, \xi_1 = 1/a_1)$ are asymptotically stable one-tangent nodes.

Thanks are due to two anonymous referees for their valuable suggestions to improve an earlier version of the manuscript. A part of this work was presented by G. H. in a lecture [7] at the Eleventh European Meeting on Cybernetics and Systems Research *organized by the Austrian Society for Cybernetics Studies, held at the University of Vienna, 21–24 April 1992. The financial support of the Biophysics Group of the Central Research Institute for Physics of the Hungarian Academy of Sciences (Budapest)*

received by G. H. is gratefully acknowledged. Many thanks are due to Harvey H. Shenker (Central Research Institute for Physics of the Hungarian Academy of Sciences) for improving the English of the manuscript.

APPENDIX. LINEAR STABILITY ANALYSIS OF THE IONE FOR SECOND-ORDER NEURONS AND PHASE FLOWS IN THE PHASE FIELD

A1. NUMERICAL DETERMINATION OF THE STATIONARY SOLUTIONS

From (13) one can obtain the relationship between the input f and the corresponding stationary solution (or singular point) ξ,

$$f(\xi) = \frac{1}{1+\Sigma_1}\left[\omega \ln\left(\frac{\xi}{1-\xi}\right) - \xi\Sigma_2\right],$$

$$\Sigma_1 = \sum_{l=1}^{M} \frac{c_l}{\varphi_l}, \qquad \Sigma_2 = \sum_{k=1}^{m} \frac{b_k}{a_k}; \qquad 0 \leqslant \xi \leqslant 1. \tag{20}$$

From a physiological point of view it is pertinent to suppose that

$$\lim_{\xi \to 0} f'(\xi) = +\infty, \qquad \lim_{\xi \to 1} f'(\xi) = +\infty,$$

$$f'(\xi) = \frac{1}{1+\Sigma_1}\left[\frac{\omega}{\xi(1-\xi)} - \Sigma_2\right], \tag{21}$$

which is satisfied if $\Sigma_1 > -1$.

If $\Sigma_2 \leqslant 0$, then $f'(\xi) > 0$ for all $\xi \in [0,1]$, so there is only one stationary solution ξ_0 for a given input f_0 (Figure 10A).

If $\Sigma_2 > 0$ and $\omega \geqslant \check{\omega}_c \equiv \Sigma_2/4$, then $f'(\xi) \geqslant 0$ for all $\xi \in [0,1]$, and $f'(1/2) = 0$, so there is only one stationary solution ξ_0 for a given input f_0 (Figures 10A and 10B).

If $\Sigma_2 > 0$ and $\omega < \check{\omega}_c$, then

$$f'(\check{\xi}_{1,2}) = 0 \quad \text{if } \check{\xi}_{1,2} = \frac{1}{2} \mp \sqrt{\frac{1}{4} - \frac{\omega}{\Sigma_2}}\,. \tag{22}$$

From Figure 10C one can read that

$$f'(\xi) > 0 \qquad \text{if } 0 \leqslant \xi < \check{\xi}_1 \quad \text{or} \quad \check{\xi}_2 < \xi \leqslant 1,$$

$$f'(\xi) < 0 \qquad \text{if } \check{\xi}_1 < \xi < \check{\xi}_2. \tag{23}$$

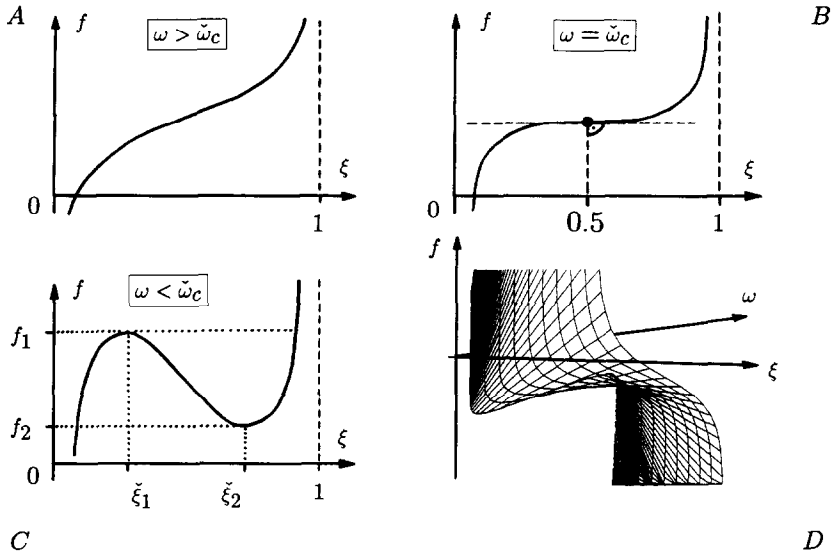

FIG. 10. Schematic representation of graph $f(\xi)$ describing the relationship between input f and the corresponding stationary solution ξ of the IONE. (A) $\omega > \check{\omega}_c$, (B) $\omega = \check{\omega}_c$, (C) $\omega < \check{\omega}_c$. (D) Three-dimensional representation of function $f(\xi, \omega)$.

Then there are three different stationary solutions if $f(\check{\xi}_2) \equiv f_2 < f_0 < f_1 \equiv f(\check{\xi}_1)$, there are two different singular points if $f_0 = f_1$ or $f_0 = f_2$, and there is only one if $f_0 > f_1$ or $f_0 < f_2$ (Figure 10C).

From (13) we obtain

$$G'(\xi) \equiv \frac{1}{\xi^2} - \frac{\Sigma_2}{\omega} \exp\left[- \frac{(1+\Sigma_1) f_0 + \xi \Sigma_2}{\omega} \right]. \tag{24}$$

Using (13) and (24), one can numerically determine ξ by means of the Newton tangent method, that is, using the recursion

$$\xi_{i+1} = \xi_i - G(\xi_i)/G'(\xi_i) \tag{25}$$

with a given initial value $\xi^{(0)}$. The three-dimensional representation of graph $f(\xi, \omega)$ is shown in Figure 10D.

A2. LINEAR STABILITY ANALYSIS OF THE IONE

In this chapter we follow Verhulst [16] in performing the linear stability analysis of the IONE.

Linearization of the IONE. The improved Oğuztöreli neural equation (6) or (12) has the following form in the stationary case:

$$-\xi + \check{S}\{(1+\Sigma_1)f + \xi\Sigma_2, \omega\} = 0, \qquad \xi_k = \xi/a_k, \qquad k = 1,\ldots,m. \tag{26}$$

Using the Taylor approximation, we obtain

$$\check{S}\{u = u_0 + x, \omega\} \equiv \frac{1}{1+e^{-(u_0+x)/\omega}} \approx \frac{1}{1+e^{-u_0/\omega}} + \frac{e^{-u_0/\omega}}{\omega(1+e^{-u_0/\omega})^2}x + \cdots. \tag{27}$$

In the vicinity of a singular point $S = (\xi, \xi_k)$ of the phase field we can write

$$X(t) = \xi + x(t), \qquad Y_k(t) = \xi_k + y_k(t),$$
$$|x(t)| \ll \xi, \qquad |y_k(t)| \ll \xi_k, \qquad k = 1,\ldots,m. \tag{28}$$

After linearization of the IONE we obtain

$$\frac{dx(t)}{dt} = -a_0 x(t) + a_0 \frac{\xi(1-\xi)}{\omega} \sum_{k=1}^{m} b_k y_k(t),$$
$$\frac{dy_k(t)}{dt} = x(t) - a_k y_k(t), \qquad k = 1,\ldots,m. \tag{29}$$

From this one can write

$$\frac{dy(t)}{dt} = \mathbf{A}y(t), \qquad \mathbf{A} = \begin{pmatrix} -a_0 & a_0 h b_1 & a_0 h b_2 & \cdots & a_0 h b_m \\ 1 & -a_1 & 0 & \cdots & 0 \\ 1 & 0 & -a_2 & \cdots & 0 \\ \vdots & \vdots & \vdots & \cdots & \vdots \\ 1 & 0 & 0 & \cdots & -a_m \end{pmatrix},$$

$$h = \frac{\xi(1-\xi)}{\omega}, \qquad y(t) = \begin{bmatrix} x(t) \\ y_1(t) \\ \vdots \\ y_m(t) \end{bmatrix}, \tag{30}$$

with the characteristic equation

$$\det(\mathbf{A} - \lambda \mathbf{I}) = 0, \tag{31}$$

where $\mathbf{I}$ is the identity matrix.

Case of Second-Order Neurons. The characteristic equation of second-order neurons with $m + 1 = 2$ is

$$\lambda^2 - T\lambda + D = 0, \tag{32a}$$

with

$$T = -(a_0 + a_1) < 0, \qquad D = a_0\left[a_1 - \frac{b_1 \xi(1-\xi)}{\omega}\right]. \tag{32b}$$

The solutions of this characteristic equation give the eigenvalues of matrix $\mathbf{A}$,

$$\lambda_{1,2} = \frac{T \pm \sqrt{T^2 - 4D}}{2}. \tag{33}$$

A3. CLASSIFICATION OF THE SINGULAR POINTS

Case $T^2 - 4D = 0$ ($T \neq 0$). This case is satisfied if

$$\omega \leqslant \tilde{\omega}_c \equiv -\frac{a_0 b_1}{(a_1 - a_0)^2} > 0 \tag{34a}$$

and

$$\xi = \tilde{\xi}_{1,2} \equiv \frac{1 \mp \sqrt{1 + \omega(a_1 - a_0)^2 / a_0 b_1}}{2} \tag{34b}$$

and

$$b_1 < 0, \tag{35a}$$

or

$$b_1 > 0 \quad \text{and} \quad a_0 = a_1 \quad \text{and} \quad \xi = 0 \quad \text{or} \quad \xi = 1. \tag{35b}$$

Then

$$\lambda_1 = \lambda_2 \equiv \lambda = T/2 < 0, \tag{36}$$

$$x(t) = (x_0 + c_1 t)e^{\lambda t}, \qquad y(t) = (y_0 + c_2 t)e^{\lambda t}, \tag{37a}$$

with

$$c_1 = \frac{a_1 - a_0}{2} c_2, \qquad c_2 = x_0 - y_0 \frac{a_1 - a_0}{2},$$
$$x_0 \equiv x(t=0), \qquad y_0 \equiv y(t=0). \tag{37b}$$

In this case the singular point $S(\xi, \xi_1)$ is an *asymptotically stable one-tangent node* (Figure 11A).

Case $T^2 - 4D > 0$ $(T \neq 0)$.

(I) $D > 0$: This case is satisfied if

$$\omega \leqslant \tilde{\omega}_c \quad \text{and} \quad b_1 < 0 \quad \text{and} \quad 0 < \xi < \tilde{\xi}_1 \quad \text{or} \quad \tilde{\xi}_2 < \xi < 1, \tag{38}$$

or

$$\omega \leqslant \breve{\omega}_c \equiv \frac{b_1}{4a_1} \quad \text{and} \quad b_1 > 0 \quad \text{and} \quad 0 < \xi < \breve{\xi}_1 \quad \text{or} \quad \breve{\xi}_2 < \xi < 1,$$
$$\breve{\xi}_{1,2} = 1/2 \mp \sqrt{1/4 - \omega a_1 / b_1}\,. \tag{39}$$

Then

$$\lambda_1 < 0, \qquad \lambda_2 < 0, \tag{40}$$

$$x(t) = c_1 e^{\lambda_1 t} + c_2 e^{\lambda_2 t}, \qquad y(t) = c_1 K_1 e^{\lambda_1 t} + c_2 K_2 e^{\lambda_2 t}, \tag{41a}$$

with

$$c_1 = \frac{y_0 - K_2 x_0}{K_1 - K_2}, \qquad c_2 = \frac{K_1 x_0 - y_0}{K_1 - K_2},$$
$$K_{1,2} = \omega \frac{a_0 - a_1 \pm \sqrt{(a_1 - a_0)^2 + 4a_0 b_1 \xi(1-\xi)/\omega}}{2a_0 b_1 \xi(1-\xi)}. \tag{41b}$$

In this case the singular point $S(\xi, \xi_1)$ is an *asymptotically stable node* (Figure 11B).

(II) $D < 0$: This case is satisfied if

$$\omega < \breve{\omega}_c \quad \text{and} \quad b_1 > 0 \quad \text{and} \quad \breve{\xi}_1 < \xi < \breve{\xi}_2. \tag{42}$$

Then

$$\lambda_1 > 0, \qquad \lambda_2 < 0 \tag{43}$$

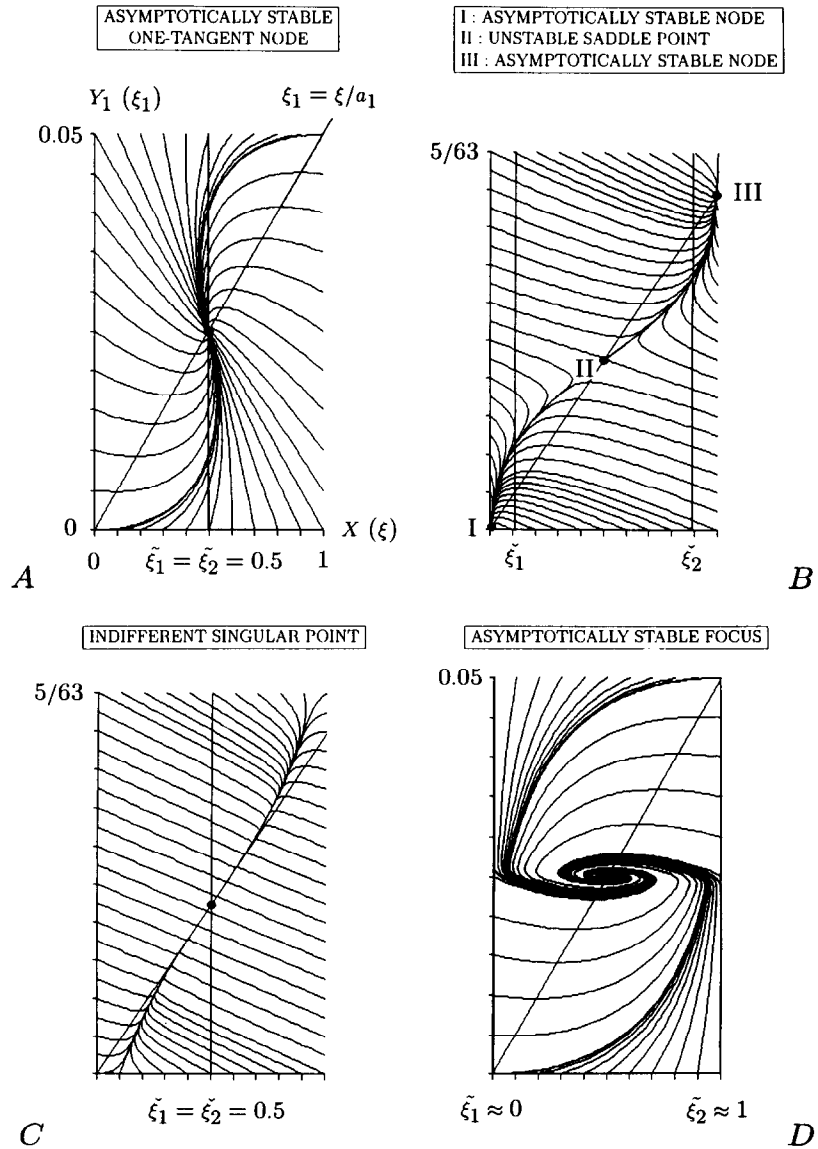

FIG. 11. Phase flows around different singular points in the phase field (X, Y_1) of the OONE. (A) Asymptotically stable one-tangent node $S(\xi = 0.5,\ \xi_1 = 0.025)$ positioned on the straight line $\xi_1 = \xi/a_1$. Parametric configuration: $a_0 = 50\ s^{-1}$, $a_1 = 20\ s^{-1}$, $b_1 = -2000\ s^{-1}$, $\omega = \tilde{\omega}_c = 111.11$, $f = 50$. (B) I, asymptotically stable node $S_I(\xi = 0.0064,\ \xi_1 = 0.0004)$; II, unstable saddle point $S_{II}(\xi = 0.5,\ \xi_1 = 0.0357)$; III, asymptotically stable node $S_{III}(\xi = 0.9935,\ \xi_1 = 0.0709)$. Parametric configuration: $a_0 = 50\ s^{-1}$, $a_1 = 14\ s^{-1}$, $b_1 = 10{,}000\ s^{-1}$, $\omega = 70$, $f = -357.1$. (C) Indifferent singular point $S(\xi = 0.5,\ \xi_1 = 0.0357)$; $a_0 = 50\ s^{-1}$, $a_1 = 14\ s^{-1}$, $b_1 = 10{,}000\ s^{-1}$, $\omega = \check{\omega}_c = 178.57$, $f = -357.1$. (D) Asymptotically stable focus $S(\xi = 0.5,\ \xi_1 = 0.025)$; $a_0 = 50\ s^{-1}$, $a_1 = 20\ s^{-1}$, $b_1 = -2000\ s^{-1}$, $\omega = 1$, $f = 50$.

with $x(t)$ and $y(t)$ as in (41a). In this case the singular point $S(\xi, \xi_1)$ is an *unstable saddle point* (Figure 11B).

(III) $D = 0$: This case is satisfied if

$$\xi = \check{\xi}_{1,2} \quad \text{and} \quad b_1 > 0 \quad \text{and} \quad \omega \leqslant \check{\omega}_c. \tag{44}$$

Then

$$\lambda_1 = 0, \qquad \lambda_2 = T < 0, \tag{45}$$

$$x(t) = c_1 + c_2 e^{\lambda_2 t}, \qquad y(t) = c_3 + c_4 e^{\lambda_2 t}, \tag{46a}$$

with

$$c_1 = a_1 \frac{x_0 + y_0 a_0}{a_0 + a_1}, \qquad c_2 = a_0 \frac{x_0 - y_0 a_1}{a_0 + a_1}, \qquad c_3 = \frac{c_1}{a_1}, \qquad c_4 = -\frac{c_2}{a_0}, \tag{46b}$$

$$y(x) = y_0 + \frac{x_0}{a_0} - \frac{x}{a_0}. \tag{47}$$

In this case the stationary solution $S(\xi, \xi_1)$ is an *indifferent singular point* (Figure 11C).

Case $T^2 - 4D < 0$ ($T \neq 0$). This case is satisfied if

$$\omega \leqslant \tilde{\omega}_c \quad \text{and} \quad b_1 < 0 \quad \text{and} \quad \tilde{\xi}_1 < \xi < \tilde{\xi}_2. \tag{48}$$

Then

$$\lambda_{1,2} = \mathrm{RE} \pm i\,\mathrm{IM}, \qquad \mathrm{RE} \equiv \frac{T}{2} < 0,$$

$$\mathrm{IM} \equiv \left[-\frac{T^2}{4} + a_0 \left(a_1 - \frac{b_1 \xi (1 - \xi)}{\omega} \right) \right]^{1/2}, \tag{49}$$

$$x(t) = A_x e^{\mathrm{RE}\, t} \sin(\mathrm{IM}\, t + \varphi_x), \qquad y(t) = A_y e^{\mathrm{RE}\, t} \sin(\mathrm{IM}\, t + \varphi_y), \tag{50a}$$

with

$$A_x = \pm \sqrt{c_1^2 + x_0^2}, \qquad A_y = \pm \sqrt{c_2^2 + y_0^2},$$

$$\varphi_x = \arctan\left(\frac{x_0}{c_1} \right), \qquad \varphi_y = \arctan\left(\frac{y_0}{c_2} \right),$$

$$c_1 = \frac{\omega x_0 (a_1 - a_0) + 2 a_0 b_1 y_0 \xi (1 - \xi)}{2 \omega\, \mathrm{IM}},$$

$$c_2 = \omega \frac{c_1 (a_0 - a_1) - 2 x_0\, \mathrm{IM}}{2 a_0 b_1 \xi (1 - \xi)}. \tag{50b}$$

In this case the singular point $S(\xi, \xi_1)$ is an *asymptotically stable focus* (Figure 11D).

Stability Regions and Phase Flows in the Phase Field

(I) If $b_1 \leqslant 0$, then $\Sigma_2 = b_1 / a_1 \leqslant 0$ is satisfied, so there is always only one stable singular point ξ_0 for a given input f_0. The singular point is positioned along the straight line $\xi_1 = \xi / a_1$ in the phase field (X, Y_1) (Figure 12). The stability character of the singular point varies in the different regions of the phase field as can be seen in Figure 12. The boundaries of these stability regions are determined by $\tilde{\xi}_{1,2}$ depending on ω.

From (34) it follows that if $a_1 \neq a_0$, then

$$\text{if} \quad \omega < \tilde{\omega}_c, \quad \text{then} \quad 0 < \tilde{\xi}_1 < 1/2; \; 1/2 < \tilde{\xi}_2 < 1, \tag{51}$$

$$\text{if} \quad \omega = \tilde{\omega}_c, \quad \text{then} \quad \tilde{\xi}_1 = \tilde{\xi}_2 = 1/2, \tag{52}$$

$$\text{if} \quad \omega > \tilde{\omega}_c, \quad \text{then} \quad \tilde{\xi}_{1,2} \in \mathbb{C}. \tag{53}$$

But if $a_1 = a_0$, then

$$\tilde{\omega}_c = +\infty \qquad \text{and} \qquad \tilde{\xi}_1 = 0; \; \tilde{\xi}_2 = 1. \tag{54}$$

If (51) is satisfied, the phase field with phase flows is represented in Figure 12. If (52) is satisfied, the central region of the asymptotically stable focus disappears, at $S(\xi = 1/2, \xi_1 = 1/2a_1)$ there is an asymptotically stable one-tangent node, and every other singular point is then an asymptotically stable node. If (53) is satisfied, the asymptotically stable one-tangent node disappears also, and every singular point is an asymptotically stable node. If (54) is satisfied, there are two asymptotically stable one-tangent nodes at the points $S_1(\xi = 0, \xi_1 = 0)$ and $S_2(\xi = 1, \xi_1 = 1/a_1)$, and every other singular point is an asymptotically stable focus.

(II) If $b_1 > 0$, then there are one, two, or three different singular points for a given input depending on f_0 and ω. The stability character of the singular points can be seen in Figure 13. The phase field consists of different stability regions, the boundaries of which are determined by $\check{\xi}_{1,2}$ depending on ω. From (39) it follows that

$$\text{if} \quad \omega < \check{\omega}_c, \quad \text{then} \quad 0 < \check{\xi}_1 < 1/2; \; 1/2 < \check{\xi}_2 < 1, \tag{55}$$

$$\text{if} \quad \omega = \check{\omega}_c, \quad \text{then} \quad \check{\xi}_1 = \check{\xi}_2 = 1/2, \tag{56}$$

$$\text{if} \quad \omega > \check{\omega}_c, \quad \text{then} \quad \check{\xi}_{1,2} \in \mathbb{C}. \tag{57}$$

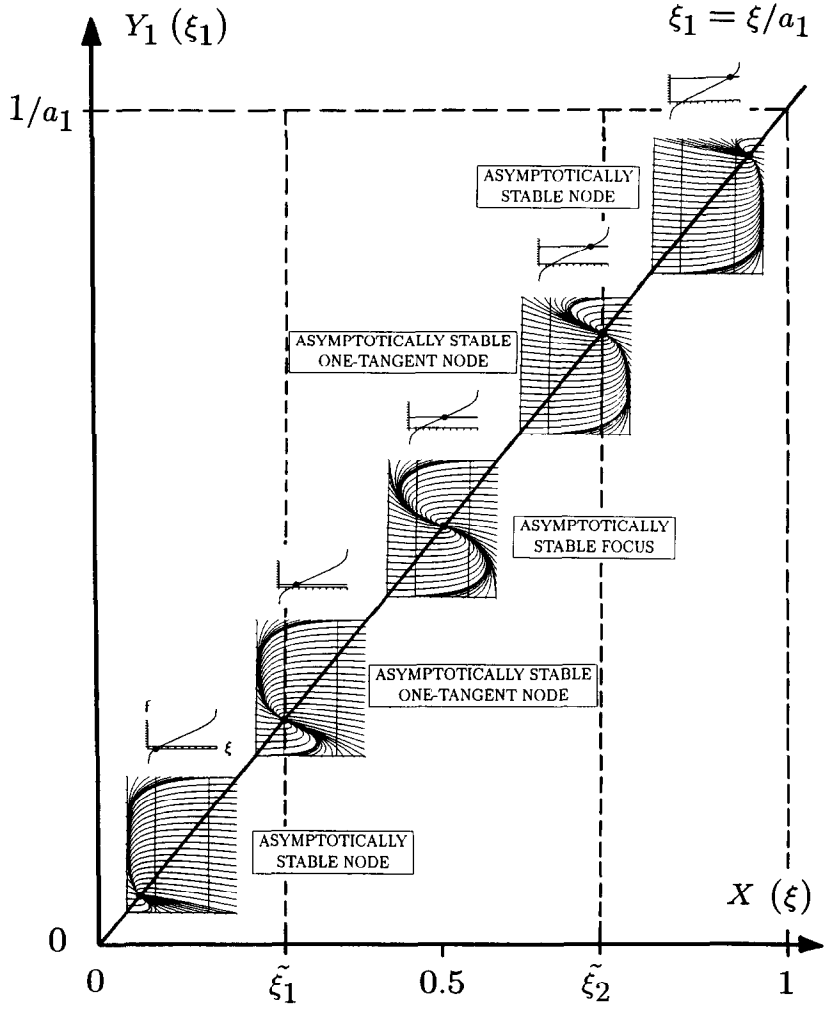

FIG. 12. Phase field (X, Y_1) of the IONE with the parametric configuration $a_0 = 100\ s^{-1}$, $a_1 = 12.5\ s^{-1}$, $b_1 = -4000\ s^{-1}$, $\omega = 40 < \tilde{\omega}_c = 52.244$, $\varphi_1 = 500\ s^{-1}$, $\varphi_2 = 12.5\ s^{-1}$, $\varphi_3 = 3.3333\ s^{-1}$, $\Phi = 8\ s^{-1}$, $\tau^* = 18$ ms. The singular point $S(\xi, \xi_1)$ for a given input f_0 is positioned on the straight line $\xi_1 = \xi/a_1$. The lower part of every inset along this line represents the phase flow around the corresponding singular point, and the upper part shows the graph $f(\xi)$. On the graph $f(\xi)$, input f_0 is represented by a horizontal line and the corresponding stationary solution by a dot.

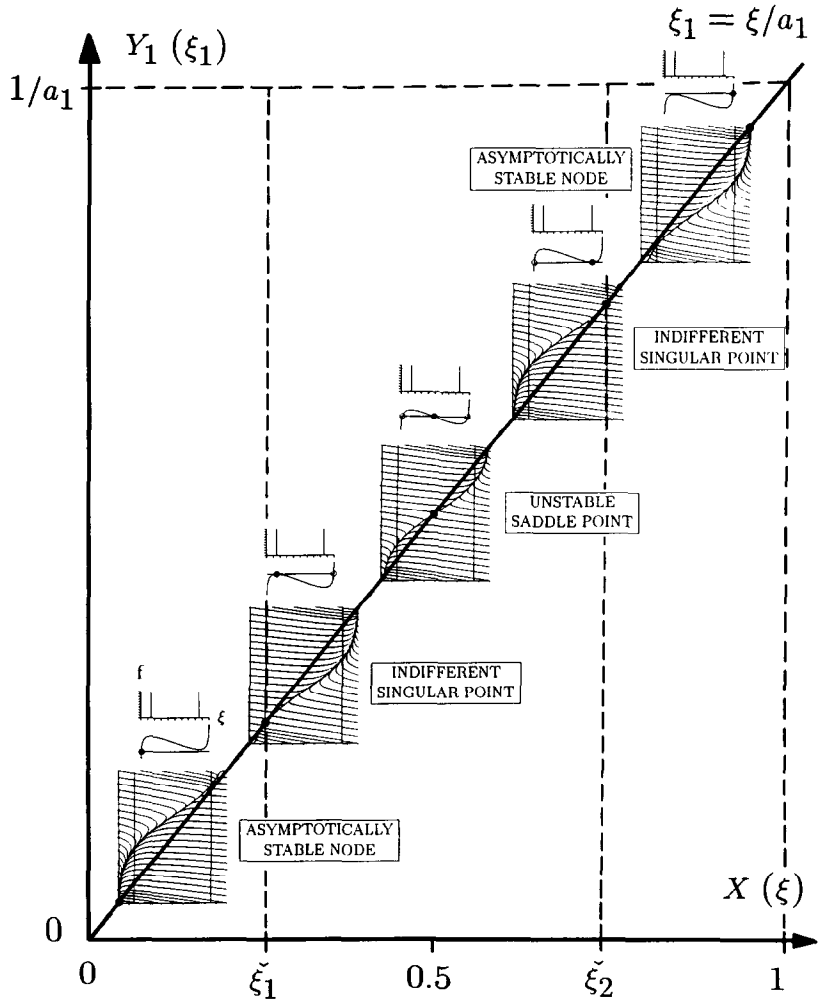

FIG. 13. Phase field (X,Y_1) of the IONE with the parametric configuration $a_0 = 100\ s^{-1}$, $a_1 = 12.5\ s^{-1}$, $b_1 = 10{,}000\ s^{-1}$, $\omega = 100 < \tilde{\omega}_c = 200$, $\varphi_1 = 500\ s^{-1}$, $\varphi_2 = 12.5\ s^{-1}$, $\varphi_3 = 3.3333\ s^{-1}$, $\Phi = 8\ s^{-1}$, $\tau^* = 18$ ms. In this case there are one, two, or three different stationary solutions for a given input f_0. In the upper part of every inset, the singular points are represented by circles. In the lower part of the insets, the phase flow belonging to the singular point, which is represented by a black circle, can be seen.

If (55) is satisfied, the phase field with phase flows is represented in Figure 13. Then there are one, two, or three different singular points depending on the value of input f_0. One can see in Figure 13 that in this case the phase field consists of a central unstable region and two peripheral stable regions. In the central region the singular points are unstable saddle points, and in the peripheral regions they are asymptotically stable nodes. At the boundaries of the stable and unstable regions the stationary solutions are indifferent singular points.

If (56) is satisfied, the central unstable region of the phase field disappears, the point $S(\xi = 1/2,\ \xi_1 = 1/2a_1)$ is an indifferent singular point, and every other stationary solution is an asymptotically stable node. If (57) is satisfied, every singular point is an asymptotically stable node. In the latter two cases there is always only one singular point for a given f_0. If $a_0 = a_1$, the singular points are $S_1(\xi = 0,\ \xi_1 = 0)$ and $S_2(\xi = 1,\ \xi_1 = 1/a_1)$, and they are asymptotically stable one-tangent nodes.

REFERENCES

1 D. Attwell, M. Wilson, and M. Samuel, A quantitative analysis of interactions between photoreceptors in the salamander (*Ambystoma*) retina, *J. Physiol.* 352:703–737 (1984).

2 J. L. Barbur, Speed discrimination and its relation to involuntary eye movements in human vision, *Neurosci. Lett.* 54:7–12 (1985).

3 J. L. Barbur, G. M. Dunn, and J. A. Wilson, The perception of moving comets at high retinal illuminance levels: a rod–cone interaction effect, *Biol. Cybern.* 55:145–158 (1986).

4 D. A. Baylor and A. L. Hodgkin, Detection and resolution of visual stimuli by turtle photoreceptors, *J. Physiol.* 234:163–198 (1973).

5 D. Burr, Motion smear, *Nature* 284:164–165 (1980).

6 B. A. Gottwald and G. Wanner, A reliable Rosenbrock integrator for stiff differential equations, *Computing* 26:355–360 (1981).

7 G. Horváth, P. Érdi, and Á. Szakál, Modelling of retinal comet-like after images, *Proceedings of the 11th European Meeting on Cybernetics and Systems Research* (Austrian Society for Cybernetics Studies, Univ. Vienna, 21–24 April 1992), R. Trappl, Ed., Vol. 1, World Scientific, Singapore, 1992, pp. 733–740.

8 B. J. Nunn and D. A. Baylor, Visual transduction in retinal rods of the monkey *Macaca fascicularis*, *Nature* 299:726–728 (1982).

9 M. N. Oğuztöreli, T. M. Caelli, and G. M. Steil, Information processing in vertebrate retina, in *Trends in the Theory and Practice of Non-Linear Analysis*, V. Lakshmikantham, Ed., Elsevier/North-Holland, Amsterdam, 1985, pp. 345–356.

10 M. N. Oğuztöreli, G. M. Steil, and T. M. Caelli, Underlying neural computations for some visual phenomena, *Biol. Cybern.* 60:89–106 (1988).

11 R. D. Penn and W. A. Hagins, Kinetics of the photocurrent of retinal rods, *Biophys. J.* 12:1073–1094 (1972).

12 J. L. Schnapf and D. A. Baylor, How photoreceptor cells respond to light, *Sci. Am.* 256(4):32–39 (1987).
13 R. B. Stein, K. V. Leung, D. Mangeron, and M. N. Oğuztöreli, Improved neural models for studying neural networks, *Kybernetik* 15:1–9 (1974).
14 R. B. Stein, K. V. Leung, M. N. Oğuztöreli, and D. W. Williams, Properties of small neural networks, *Kybernetik* 14:223–230 (1974).
15 L. Stryer, The molecules of visual excitation, *Sci. Am.* 257(1):32–40 (1987).
16 F. Verhulst, *Nonlinear Differential Equations and Dynamical Systems*, Springer Verlag, New York, 1990, p. 277.